MAGNETIC RESONANCE IN MEDICINE

# New Method for Contrast Manipulation in DNP-Enhanced MRI

Gorazd Planinšič, Daniel Grucker, Janez Stepišnik

**The magnetization subtraction technique (MS), which is equivalent to the inversion recovery technique in strong magnetic fields, has been implemented in dynamic nuclear polarization-enhanced magnetic resonance imaging (DNPI). The general theoretical basis of the MS method, which can be applied to DNPI or to prepolarized MRI in weak magnetic fields (such as Earth's magnetic field), is introduced. Details are provided about the signal amplitude, dynamic range of the method, and conditions required to observe signal void in samples with specific $T_1$ relaxation times. The experimental results obtained with MS DNPI are presented and discussed. In the experiments, electron spin resonance irradiation frequencies of 199 MHz and 16.2 MHz were employed. Also, $T_1$ contrast manipulation in the polarizing and in the detection magnetic field is discussed and demonstrated for MS DNPI.**

**Key words: MR imaging; contrast manipulation; DNP; Overhauser's enhancement.**

## INTRODUCTION

Weak-field MRI methods have the common feature that the polarization of the sample and signal detection are performed under different conditions. In most cases, the detection magnetic field, $B_d$, alone is not strong enough to produce a useful magnetization of the sample. For this reason, no magnetization recovery can be observed in weak fields, as it does in inversion recovery (IR) sequences in strong magnetic fields. However, zero-crossing of the magnetization for a particular longitudinal relaxation time, $T_1$, similar to the phenomenon observed in IR sequences, can be achieved also in weak fields. The basic idea is to employ two polarization periods with a polarizing field in the same direction. Between these two polarizations, the direction of the sample magnetization is inverted by application of a 180° pulse. The second polarization, depending on its duration, initially decreases and then subsequently increases the sample magnetization, very much like the effect of the 180° − 90° time interval in the IR technique. We have named this technique magnetization subtraction (MS). Its main advantage is in the possibility of $T_1$-contrast manipulation in weak-field MRI experiments. Remembering that differences between the $T_1$ of different biological tissues become significantly larger in weak magnetic fields (1, 2) makes the ability of contrast manipulation in weak-field MRI even more attractive. Magnetization subtraction was first applied in our experiments with Earth's magnetic field (3) and presented recently (4), but without detailed theoretical treatment.

In our experiments, we had used dynamic nuclear polarization-enhanced MRI (DNPI), an imaging method that became popular over the past five years due to its interesting potential for medical applications (5–9). In these experiments, DNPI was used as a proton–electron double resonance technique, where the nuclear magnetization of the sample containing a free radical, is increased by saturation of the electron resonance (10–12). The aim of this work was to apply the idea of MS to DNPI, and to give a general theoretical treatment of the MS technique in weak magnetic fields.

## MATERIAL AND METHODS

All DNPI experiments were performed on a Bruker imaging system, with facilities for static magnetic field cycling, and conversion of NMR receive/transmit frequency between 289 kHz and 10.711 MHz. The main magnetic field was generated by the resistive air core split-solenoid, and field cycling was performed with an adapted gradient power supply. Gradient and shim fields were generated by standard Bruker coils (inside diameter, 31 cm). Nuclear magnetic resonance signal detection was performed at 68 G (289 kHz). Electron spin resonance (ESR) irradiation frequencies of 199 MHz and 16.2 MHz were used and were generated by a 40-W and 30-W power amplifier, respectively. The ESR irradiation field was always perpendicular to the direction of the main magnetic field. All DNPI experiments were performed on phosphate-buffered solutions of the nitroxide 2,2,6,6-tetramethyl-4-oxo-piperidine-*N*-oxyl (Aldrich Co.), referred to as TXO.

In all weak-field MRI methods, relatively high-inductance NMR coils have to be used for the detection of low Larmor frequencies. Switching the high-inductance coils causes transients that impair the quality of NMR pulses. For this reason, the setup with separate transmit and receive NMR coils is advantageous in weak-field MRI.

## THEORY

The signal amplitude after an MS sequence can be calculated using the Bloch equations. The calculation is a little more complex than the calculations for IR sequences because most weak-field MRI methods involve switches of constant magnetic field. In practice, this requires ring-down delays after every change of magnetic field, taking into account the $T_1$ field-dependence also. In this paragraph, the proton magnetization after MS is

MRM 35:379–383 (1996)

From the Fakulteta za matematiko in fiziko, Univerza v Ljubljani, Ljubljana, Slovenia (G.P., J.S.) and Institute de Physique Biologique, Strasbourg, France (D.G.).

Address correspondence to: G. Planinšič, Ph.D., Oddelek za Fiziko, Univerza v Ljublani, Jadranska 19, 61000 Ljubljana, Slovenia.

Received March 1, 1995; revised September 11, 1995; accepted September 18, 1995.

0740-3194/96 $3.00

calculated for DNPI and for prepolarized MRI in weak magnetic fields (such as Earth's magnetic field).

### DNP-Enhanced MRI

The free-radical solution can be treated as a two-spin system with proton spins coupled to electron spins. In such a system, any deviation from the equilibrium population of the electron levels produces a change in the nuclear polarization. A consequential enhancement of the nuclear polarization (therefore, of the NMR signal) may be observed in a free-radical solution if the correct electron transition is saturated before the 90° pulse. The deviation from equilibrium nuclear magnetization due to DNP is usually expressed by Overhauser's enhancement Factor $A$:

$$A = \frac{M_A}{M_P} - 1, \qquad [1]$$

where $M_A$ is the maximum magnetization that can be achieved by given DNP enhancement in the polarizing field $B_p$, and $M_p$ is the equilibrium magnetization in the same field. Enhancement Factor $A$ can be determined experimentally by measuring the NMR signals in $B_p$ with and without ESR irradiation.

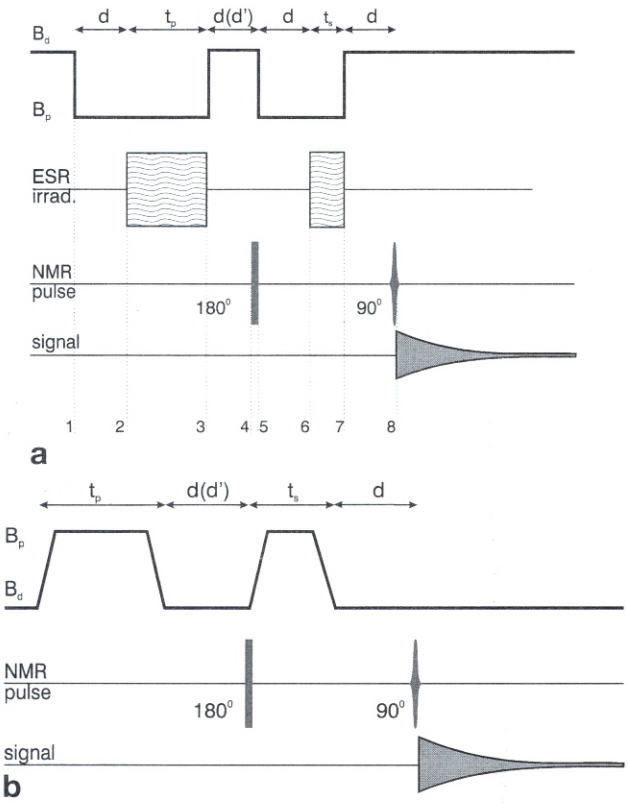


FIG. 1. (a) The preparation part of pulse sequence for MS DNPI experiment. (b) the preparation part of pulse sequence for MS in prepolarized MRI in the weak magnetic field. The applications of gradients are as in conventional MRI and are not shown in the figure. The $T_{1d}$ contrast manipulation is achieved by varying the second ESR irradiation time, $t_s$. The $d$–$s$ are ring-down delays and $d'$ is the variable time delay when the sequences are used for $T_{1p}$ contrast manipulation.

Enhanced magnetization $M_A$ can point in the direction of $B_0$ or in the opposite direction. The sign of $M_A$ depends on the nature of the electron–proton interaction, and, in weak fields, also on how electron wave functions are mixed as a result of the hyperfine coupling between electrons and nuclei. In a very weak polarizing field, $B_p$, it is practically impossible to measure the nonenhanced NMR signal (which is proportional to $M_p$). However, in field cycling experiments the detection field, $B_d$ is usually larger than the polarizing field $B_p$, therefore, the nonenhanced NMR signal may be measurable in the detection field. In this case, it is more convenient to define the enhancement factor as:

$$E = \frac{M_A}{M_d}, \qquad [2]$$

which is related to Overhauser's enhancement factor defined in Eq. [1] by the expression

$$A = E\frac{B_d}{B_p} - 1. \qquad [3]$$

Figure 1a shows a typical MS sequence for DNPI. The applications of gradients are as in conventional MRI and are not shown in the figure. Let us assume that the magnetization decay is monoexponential, with the relaxation times $T_{1p}$ and $T_{1d}$ ($T_1$ in $B_p$ and $B_d$, respectively) and initial magnetization is equal to $M_d$ (i.e., long repetition time). In this case, the following expressions for time evolution of magnetization during MS sequence in DNPI can be obtained

$$\begin{aligned} M_1 &= M_d \\ M_2 &= M_p(1 - U_p) + M_1U_p \\ M_3 &= M_A(1 - V) + M_2V \\ M_4 &= M_d(1 - U_d) + M_3U_d \\ M_5 &= -qM_4 \\ M_6 &= M_p(1 - U_p) + M_5U_p \\ M_7 &= M_A(1 - X) + M_6X \\ M_8 &= M_d(1 - U_d) + M_7U_d \end{aligned} \qquad [4]$$

where

$$U_p = \exp\left(-\frac{d}{T_{1p}}\right), \quad U_d = \exp\left(-\frac{d}{T_{1d}}\right), \quad V = \exp\left(-\frac{t_p}{T_{1p}}\right), \quad X = \exp\left(-\frac{t_S}{T_{1p}}\right) \qquad [5]$$

and the meaning of time intervals is indicated in Fig. 1a. The constant $q$ describes the quality of 180° pulse. The $q$ can be estimated by

$$q = \sqrt{1 - \left(\frac{S_{180}}{S_{90}}\right)^2}, \qquad [6]$$

where $S_{180}$ and $S_{90}$ are signal amplitudes after 180° and after 90° pulses, respectively. Using simple algebra, the

magnetization $M_8$, which is proportional to NMR signal amplitude after the 90° pulse, can be expressed as follows:

$$M_8 = M_A U_d(1 - X - qXU_dU_p + qXU_dU_pV) + M_d(1 - U_d + qXU_d^2U_p - qXU_dU_p - qXU_d^2U_p^2V) + M_pXU_d(1 - U_p + qU_dU_p^2V - qU_dU_pV). \quad [7]$$

Two particular cases were examined. In the first case, $B_d$ is equal to $B_p$ (no field cycling). Because there is no switching of main magnetic field in this case, the ring-down delay, $d$, can be considerably shortened, and Eq. [7] is simplified by setting $U_d = U_p = 1$:

$$M_8 = M_A\left(1 - X\left(1 + q - qV + \frac{1}{E}qV\right)\right). \quad [8]$$

Note that with perfect 180° pulse ($q = 1$) and complete initial polarization ($V = 0$), $M_8$ is equal to $M_A(1 - 2exp(-t_s/T_{1p}))$, which is exactly the result obtained for IR in strong magnetic fields. For substantial DNP enhancement ($|E| \gg 1$), the term $E - 1qV$ in Eq. [8] can be left out, making the signal after MS sequence equal to

$$S = S_A(1 - X(1 + q(1 - V))), \quad [9]$$

where $S_A$ is NMR free induction decay signal obtained with an ESR irradiation time longer than 5 $T_1$. Using Eq. [9], it is possible to estimate the duration of the second ESR irradiation, required to get zero signal (the condition to obtain signal void in a part of the sample with a particular $T_1$)

$$t_{S0} = T_1 \ln(1 + q(1 - V)). \quad [10]$$

The dynamic range of the method, i.e., the difference between the largest positive and largest negative signal (i.e., $t_s = 0$ and $t_s > 5\ T_1$, respectively) is given by

$$\Delta S = S_A(1 + q(1 - V)) \leq 2S_A \quad [11]$$

In the second case, we considered DNPI experiments with field cycling. In this imaging method, the main magnetic field is switched to a lower value during ESR irradiation. This is the usual way that the ESR frequency and related sample heating are reduced (13) and how DNPI experiments in very low magnetic field are performed (13–16). Instances of significant enhancement ($|E| \gg 1$) in weak polarization field ($B_p \ll B_d$) are of particular interest. In this cases, the second and the third line in Eq. [7] can be left out, giving the expression

$$M_8 = M_A U_d(1 - X(1 + qU_dU_p(1 - V))) \quad [12]$$

from which the condition for signal void and the dynamic range are calculated

$$t_S = T_{1p} \ln(1 + qU_dU_p(1 - V)), \quad [13]$$

$$\Delta S = S_A U_d(1 + qU_dU_p(1 - V)). \quad [14]$$

As expected, the dynamic range in this case is narrower due to the signal decay during ring-down delays (compare Eqs. [11] and [14]). Note that by changing the duration of the second ESR irradiation it is possible to achieve $T_{1p}$ contrast manipulations in DNPI. By measuring the signal amplitude versus the duration of second ESR irradiation, the longitudinal relaxation time $T_{1p}$ of the sample can be determined.

The same pulse sequence can be used also for $T_{1d}$ contrast manipulations ($T_{1d}$ measurement). By keeping $t_s$ (therefore, $X$) constant and changing the delay, $d$, in the magnetic field $B_d$ before applying the 180° pulse, the typical zero-crossing can also be achieved. To realize this, Eq. [12] should be rearranged as follows:

$$M_8 = M_A U_d((1 - X) - U'_d qXU_p(1 - V)) \quad [15]$$

where

$$U'_d = \exp\left(-\frac{d'}{T_{1d}}\right) \quad [16]$$

and $d'$ is the variable time delay. But, because $d'$ cannot be shorter than ring-down delay $d$, the dynamic range for $T_{1d}$ MS method is equal to

$$\Delta S = S_A U_d^2 U_p qX(1 - V). \quad [17]$$

The optimal parameter $X$ can be estimated from the additional requirement that the extreme negative and positive signals have the same magnitude, giving

$$X_{op} = \frac{1}{1 + \frac{1}{2}qU_dU_p(1 - V)}. \quad [18]$$

Combining Eqs. [17] and [18], the dynamic range for $T_{1d}$ MS method is given by

$$\Delta S = S_A \frac{U_d^2 U_p q(1 - V)}{1 + \frac{1}{2}qU_dU_p(1 - V)} \leq \frac{1}{3}2S_A, \quad [19]$$

from which it is evident that even under the ideal conditions, only one-third of the dynamic range for $T_{1p}$ MS method (Eqs. [11] and [14]) can be reached.

## Prepolarized MRI in Weak Magnetic Field

Figure 1b shows a typical MS sequence for prepolarized MR experiment in weak magnetic field. The sample is prepolarized in relatively strong polarizing field $B_p$, which is then switched down to a very weak detection field $B_d$ (about 0.5 G for Earth's magnetic field). The orientation of the coil setup is such that $B_p$ is perpendicular to $B_d$. In contrast to DNPI, this method does not require the use of chemical agents. The signal arises from the magnetization of the sample that builds up while $B_p$ is applied. Adiabatic switches are the important mechanism of spin manipulation in this method. Theory shows that during an adiabatic switch-off of $B_p$ the net magnetization of the sample turns in the direction of the residual field $B_d$. The 90° and 180° pulses of oscillating magnetic field are applied in the direction perpendicular to $B_d$.

Although the orientation of the magnetization of the sample changes between two perpendicular directions, the time evolution of magnetization can be calculated in the same way as for MS DNPI. By comparing the two sequences (Figs. 1a and 1b), it easy to see that the latter

can be obtained from the former with the substitution of $M_A$ by $M_p$ and with $d = 0$ (i.e., $U_p = 1$). Because in this method, $B_p \gg B_d$, the terms in Eq. [7] containing $M_d$ can be left out, and the expression for the magnetization after MS sequence, shown in Fig. 1b, can be written as follows

$$M = M_p U_d(1 - X(1 + qU_d(1 - V))). \quad [20]$$

The conditions for signal void and the dynamic range are calculated from Eq. [20]

$$t_{S0} = T_{1p} \ln(1 + qU_d(1 - V)), \quad [21]$$

$$\Delta S = S_A U_d(1 + qU_d(1 - V)). \quad [22]$$

Note again that the method enables $T_{1p}$ contrast manipulation. By rearranging Eq. [20] as

$$M = M_A U_d((1 - X) - qU'_d(1 - V)), \quad U'_d = \exp\left(-\frac{d'}{T_{1d}}\right), \quad [23]$$

one can see that the zero-crossing of magnetization can also be achieved by keeping the duration of second magnetization constant and changing the time interval $d'$ between two magnetizations. This would result in $T_{1d}$ contrast manipulations. Calculations similar to those used for DNPI show that the dynamic range, in this case, is again less than one-third of the dynamic range given by Eq. [17], making this version of MS in weak magnetic fields less interesting.

## RESULTS

Figure 2 shows the MS DNP-enhanced images for different $t_s$ values. These images were obtained at 68 G, without field cycling and with ESR frequency of 199 MHz. The Overhauser enhancement was obtained by saturating the central ESR line of TXO (i.e., transition $T_{25}$ defined in ref. 16). The images obtained with field cycling are shown in Fig. 3. In this case, the static magnetic field was switched between 14 G (during ESR irradiation at 16.2 MHz) and 68 G (during detection of the NMR signal). The Overhauser enhancement was obtained by saturating the ESR line corresponding to transition $T_{34}$, defined in ref. 16. In the first experiment, the phantom consisted of three 25-ml bottles, and in the second, of five 14-ml bottles. All the bottles contained TXO solution at various concentrations, and were arranged as shown on Figs. 2 and 3. In all cases we used a first ESR irradiation of 1.5 s and repetition time of 2 s. Imaging was performed on a 64 × 64 matrix, with and without slice selection, typically with eight averages, in about 30 min. A signal void and contrast inversion were observed for every sample. However, some deviations from typical inversion-recovery results were noted. Figures 2 and 3 show that several bottles may be nulled out simultaneously though they contain solutions at different free-radical concentrations. The reason for this is that, in MS sequences, the signal amplitude depends on $T_1$ relaxation times and on the enhancement factor $E$, and both quantities happen to vary with the free-radical concentration, $c$. It is well known that $1/T_1$ is roughly proportional to $c$. The dependence of $E$ on $c$ is more complex and further depends on the ESR irradiation frequency. With an ESR irradiation frequency of 199MHz, $E(c)$ has a maximum at 3mM TXO concentration. This explains why the contrasts of 1mM and 2mM samples in Fig. 2 are almost equal. On the other hand, we measured that, with an ESR frequency of 16.2MHz, $E$ is roughly proportional to $c$ for the concentrations used in this experiment. This can account for the unusual contrast behavior in Fig. 3. Table 1 shows the

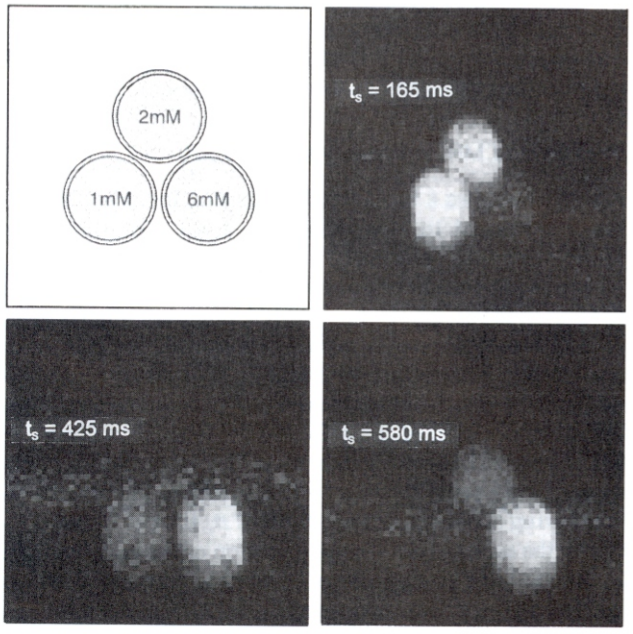


FIG. 2. The results of contrast manipulation using MS DNPI on a phantom (no field cycling, magnetic field 68 G, ESR irradiation frequency 199 MHz, image matrix 64 × 64, no slice selection, eight averages).

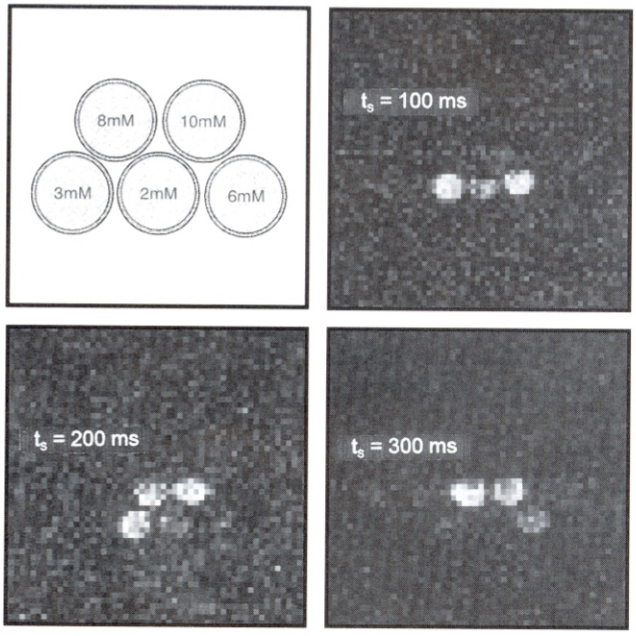


FIG. 3. The results of contrast manipulations using MS DNPI on a phantom (field cycling, polarizing magnetic field 14 G and detection field 68G ESR irradiation frequency 16.2 MHz, image matrix 64 × 64, slice thickness 20 mm, 10 averages).

Table 1
Measured enhancement factors ($E$), $T_1$ relaxation times, 180° pulse quality factors ($q$), and calculated $t_{s0}$ values for MS in DNPI[a]

| | $E$ | $T_{1p} = T_{1d}$ [ms] | $q$ | $t_{s0}$ [ms] |
|---|---|---|---|---|
| ESR freq. 16.2 MHz ($t_p$ = 1.5 s, d = 100 ms) | | | | |
| 6 mM | −8.5 | 400 ± 50 | 0.85 ± 0.05 | 160 ± 55 |
| 3 mM | −6.5 | 700 ± 50 | 0.85 ± 0.05 | 310 ± 40 |
| | $E$ | $T_1$ [ms] | $q$ | $t_{s0}$ [ms] |
| ESR freq. 199 MHz ($t_p$ = 1.5 s, d = 100 ms) | | | | |
| 6 mM | −20 | 400 ± 50 | 0.88 ± 0.05 | 170 ± 60 |
| 2 mM | −25 | 930 ± 50 | 0.88 ± 0.05 | 420 ± 40 |

[a] No difference between $T_{1p}$ and $T_{1d}$ values for TXO solutions in 14 and 68 G was observed.

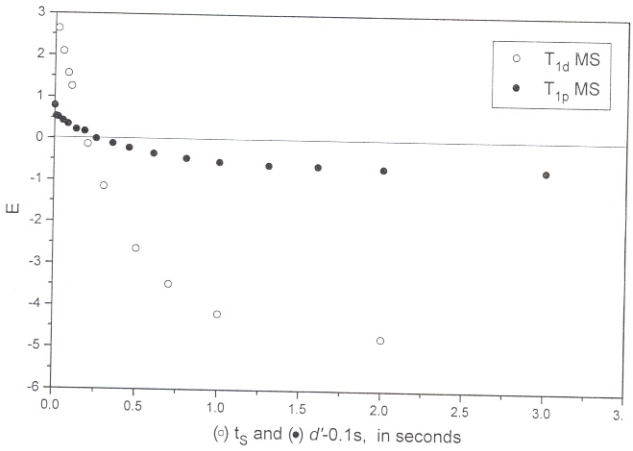


FIG. 4. Comparison of $T_{1\rho}$ and $T_{1d}$ MS methods. The measurements were performed in 14-G polarizing field, with an ESR irradiation frequency of 16.2 MHz, on agarose sample with added TXO solution. The signal was normalized to the NMR signal in the detection field (68 G). The second ESR polarization time, $t_s$, was set to 130 ms during $T_{1\rho}$ MS measurements. To present both measurements on the same graph the 100-ms ring-down delays were subtracted from $d'$ in $T_{1\rho}$ MS method.

calculated $t_{s0}$ values for two samples taken from each experiment.

As we have already mentioned in the theoretical section, the same MS sequence can be also used for $T_{1d}$ contrast manipulation. The comparison of the results obtained with the $T_{1\rho}$ and $T_{1d}$ MS methods on agarose samples with added TXO solution (Fig. 4) clearly shows the poor dynamic range of the latter method.

## CONCLUSIONS

The theoretical treatment of the general MS technique has been presented for applications to DNP-enhanced MRI and prepolarized MRI in magnetic fields as weak as Earth's magnetic field. Our experiments confirmed that MS is useful $T_1$ contrast manipulation method for DNPI. On all the images, shifts in signal void were clearly visible, depending on the second ESR irradiation duration. Observed and calculated $t_{s0}$ values show a good correlation. In addition, it has been shown, theoretically and experimentally, that where field-cycling experiments are concerned, the same method can be applied for $T_1$ measurements in the polarizing and detection magnetic fields. However, the dynamic range of the latter is considerably lower. It is also worth noticing that field-cycling DNP-enhanced images were obtained using an ESR irradiation frequency as low as 16.2 MHz. To the best of our knowledge this is the lowest ESR irradiation frequency used in DNPI so far. Low ESR irradiation frequency is of high importance for potential *in vivo* DNPI applications, because RF power absorption in biological tissues is proportional to the square of the frequency. However, future *in vivo* DNPI applications will depend also on development of new free radicals that give reasonable enhancement at lower concentrations.

## REFERENCES

1. S. H. Koenig, D. Adams, D. Emerson, C. G. Harrison, Magnetic field dependence of 1/T1 of protons in tissue, Research Report RC 10116, IBM Research Division, (1983).
2. S. H. Koenig, W. E. Schillinger, Nuclear magnetic relaxation dispersion in protein solutions. *J. Biol. Chem.* **244,** 3283–3289 (1969).
3. G. Planinšič, "Imaging of Relaxation Time Spatial Distribution by MR in Very Weak Magnetic Field," Ph.D. thesis, Univerza v Ljubljani, Ljubljana, 1993.
4. G. Planinšič, J. Stepišnik, M. Kos, Relaxation-time measurement and imaging in the Earth's magnetic field. *J. Magn. Reson.* **A110,** 170–174 (1994).
5. D. Lurie, D. M. Bussel, L. H. Bell, J. R. Mallard, Proton-electron double magnetic resonance imaging of free radical solutions. *J. Magn. Reson.* **76,** 366–370 (1988).
6. D. Grucker, In vivo detection of injected free radicals by Overhauser effect imaging. *Magn. Reson. Med.* **14,** 140–147 (1990).
7. D. Lurie, I. N. Nicholson, M. A. Foster, J. R. Mallard, Free radicals imaging in vivo in the rat by using proton–electron double resonance imaging. *Phil. Trans. R. Soc. Lond.* **A333,** 453–456 (1990).
8. D. Grucker, J. Chambron, Oxygen imaging in perfused hearts by dynamic nuclear polarisation. *Magn. Reson. Imaging* **11,** 691–696 (1993).
9. D. Grucker, Proton imaging after dynamic polarization, *in* "Magnetic Resonance Spectroscopy" (B. Bluemich, W. Khun, Eds.), pp. 573–585, VCH Weinheim, 1992.
10. I. Solomon, Relaxation processes in a system of two spins. *Phys. Rev.* **99,** 559–565 (1955).
11. R. A. Dwek, R. E. Richards, D. Taylor, Nuclear electron double resonance in liquids. *Annu. Rev. NMR Spectrosc.* **2,** 293–344 (1969).
12. W. Muller-Warmuth, K. Meise-Gresch, Molecular motions and interactions as studied by dynamic nuclear polarisation (DNP) in free radicals. *Adv. Magn. Reson.* **11,** 1–45 (1983).
13. D. Lurie, J. M. S. Hutchison, L. H. Bell, I. Nicholson, D. M. Bussell, J. R. Mallard, Field-cycling PEDRI of free radicals in large aqueous samples. *J. Magn. Reson.* **84,** 431–437 (1989).
14. R. Besson, H. Lemaire, A. Rassat, P. Servoz-Garvin, *in* "Electron Magnetic Resonance and Solid Dielectrics," Compte Rendu XIIe colloque AMPERE, Bordeaux (R. Servan, A. Charru, Eds.), pp. 327–333, Amsterdam, North-Holland, 1964.
15. T. Guiberteau, "Dynamic Nuclear Polarization in Weak Magnetic Field: Application to Spectroscopy and Oxymetry," Ph.D. thesis, Universite Louis Pasteur de Strasbourg, Strasbourg, 1994.
16. T. Guiberteau, D. Grucker, Dynamic nuclear polarisation of water protons by saturation of $\pi$ and $\sigma$ transitions of nitroxides. *J. Magn. Reson.* **A105,** 98–103 (1993).